Synthesis and testing of novel alternative oxidase (AOX) inhibitors with antifungal activity against *Moniliophthora perniciosa* (Stahel), the causal agent of witches' broom disease of cocoa, and other phytopathogens

Running title: new AOX inhibitors with antifungal activity

Mario RO Barsottini[1,2], Bárbara A Pires[1], Maria L Vieira[2], José GC Pereira[2], Paulo CS Costa[2,3], Jaqueline Sanitá[2], Alessandro Coradini[1], Fellipe Mello[1], Cidnei Marschalk[1], Eder M Silva[4], Daniele Paschoal[4], Antonio Figueira[4], Fábio HS Rodrigues[5], Artur T Cordeiro[2], Paulo CML Miranda[3], Paulo SL Oliveira[2], Maurício L Sforça[2], Marcelo F Carazzolle[1], Silvana A Rocco[2], Gonçalo AG Pereira[1,*]

[1] Genomics and bioEnergy Laboratory, Institute of Biology, State University of Campinas, Campinas, Brazil

[2] Brazilian Biosciences National Laboratory, Brazilian Center for Research in Energy and Materials, Campinas, Brazil

[3] Institute of Chemistry, State University of Campinas, Campinas, Brazil

[4] Center for Nuclear Energy in Agriculture, University of Sao Paulo, Piracicaba, Brazil

[5] Current address: School of Life Sciences, University of Warwick - Gibbet Hill Campus, Coventry, United Kingdom

[*]Corresponding author

E-mail: goncalo@unicamp.br (GAGP)

Abstract

BACKGROUND: *Moniliophthora perniciosa* (Stahel) Aime & Phillips-Mora is the causal agent of witches' broom disease (WBD) of cocoa (*Theobroma cacao L.*) and a threat to the chocolate industry. The membrane-bound enzyme alternative oxidase (AOX) is critical for *M. perniciosa* virulence and resistance to fungicides,

This article has been accepted for publication and undergone full peer review but has not been through the copyediting, typesetting, pagination and proofreading process, which may lead to differences between this version and the Version of Record. Please cite this article as doi: 10.1002/ps.5243

which has also been observed in other phytopathogens. Notably AOX is an escape mechanism from strobilurins and other respiration inhibitors, making AOX a promising target for controlling WBD and other fungal diseases.

RESULTS: We present the first study aimed at developing novel fungal AOX inhibitors. *N*-Phenylbenzamide (NPD) derivatives were screened in the model yeast *Pichia pastoris* through oxygen consumption and growth measurements. The most promising AOX inhibitor (NPD 7j-41) was further characterized and displayed better activity than the classical AOX inhibitor SHAM *in vitro* against filamentous fugal phytopathogens, such as *M. perniciosa*, *Sclerotinia sclerotiorum* and *Venturia pirina*. We demonstrate that 7j-41 inhibits *M. perniciosa* spore germination and prevents WBD symptom appearance in infected plants. Finally, an structural model of *P. pastoris* AOX was created and used in ligand structure activity-relationships analyses.

CONCLUSION: We present novel fungal AOX inhibitors with antifungal activity against relevant phytopathogens. We envisage the development of novel antifungal agents to secure food production.

Keywords: Witches' broom disease; Moniliophthora perniciosa; Alternative oxidase; fungicide; crop protection; structure activity relationship (SAR).

1. Introduction

Moniliophthora perniciosa (Stahel) Aime & Phillips-Mora is the causal agent of the witches' broom disease (WBD) of cocoa (*Theobroma cacao* L.) and a major threat to the multi-billion dollar industry of chocolate production and commercialization. Present in the Americas, this basidiomycete fungus is responsible for a Brazilian crisis after an outbreak in the largest cocoa-producing state (Bahia) in 1989. *M. perniciosa* also risks reaching Africa, where cocoa varieties highly susceptible to WBD are widely used. Thus far, there is no method to eradicate *M. perniciosa* from affected areas and farmers rely upon resistant cacao clones and crop management techniques to reduce WBD's impact[1,2].

M. perniciosa is a hemibiotrophic pathogen, and WBD is divided in biotrophic and necrotrophic phases. The biotrophic phase starts when basidiospores infect meristems (shoots, flower buds and young fruits) and develop into sparsely growing hyphae inside of the plant organs. This is when crucial host-pathogen interactions occur and lasts 2-3 months, which is unusually long for a phytopathogen. Afterwards, the infected cocoa tissues whiter, which hallmarks the start of the necrotrophic phase, and a dense *M. perniciosa* mycelium grows on dead cocoa tissues. The transition between the biotrophic and necrotrophic WBD phases correlate with extensive morphophysiological changes in *M. perniciosa*. Notably, we have identified that the mitochondrial enzyme alternative oxidase (AOX) is exclusively expressed during the biotrophic phase and plays a critical role for *M. perniciosa* virulence as well as survival to fungicides[3,4].

AOX is widely distributed among organisms, being found in bacteria, yeasts, fungi, protists, plants and animals[5,6]. It is a membrane protein located in the matrix side of the inner mitochondrial membrane and creates a branching point in the electron transport chain (ETC) at the ubiquinone level. AOX reduces oxygen to water without the engagement of complexes III and IV, thus providing metabolic plasticity to the cell to, among other things, cope with biotic and abiotic stress[7–10]. Here, we highlight AOX as a resistance factor to ETC inhibitors and fungicides, notably strobilurins and Q_O inhibitors[11,12].This has been shown in a number of phytopathogens that attack several important crops worldwide, such as *Magnaporthe grisea*[13], *Moniliophthora perniciosa*[3], *Mycosphaerella graminicola*[14,15], *Sclerotinia sclerotiorum*[16] and *Venturia inaequalis*[17], among others[18–21].

Derivatives of gallic acid and hydroxamic acid are long known AOX inhibitors, but they have poor pharmacological properties and are not adequate for commercial use[19,22]. Ascofuranone and structural analogues are potent inhibitors of the human parasite *T. brucei* AOX (TAO)[23,24], and current efforts are directed towards improving the pharmacological properties of TAO inhibitors for clinical use[25–27]. However, comprehensive studies on fungal AOX inhibition are scarce, and structure-based drug design of compounds targeting other organisms is limited by the fact that the sole AOX structure available thus far is from TAO. Moreover, synthesizing ascofuranone and derivatives is laborious and demands several reactional steps, which reduces yield and increases cost. In spite of current advances in computational biology, it is imperative to obtain experimental data to direct drug design initiatives targeting fungal AOXs.

Here, we describe a novel class of easily synthesized AOX inhibitors with antifungal activity. *Pichia pastoris* is a robust yeast used for industrial applications that grows aerobically and contains an AOX gene. *P. pastoris* was thus employed to evaluate 74 rationally designed *N*-Phenylbenzamide derivatives (NPD) through measurements of oxygen uptake and growth, providing information on potency, selectivity and antifungal potential of those compounds. The most potent and selective NPD (7j-41) was then tested against filamentous fungal phytopathogens *M. perniciosa*, *S. sclerotiorum* and *Venturia pirina*, and the three species displayed sensitivity to 7j-41. We further demonstrate that 7j-41 prevents *M. perniciosa* basidiospore germination *in vitro*, as well as the development of WBD symptoms in infected plants. An experimentally-validated structural model of *P. pastoris* AOX is presented, which enabled analyses of structure-activity relationship for the tested NPD library. We envisage that our results will be useful for the study of fungal AOXs, as well as for the development of novel antifungal agents based on AOX inhibitors.

2. Materials and Methods

2.1. Reagents and respiration inhibitors.

Respiration inhibitors used in this work were potassium cyanide, salicylhydroxamic acid (SHAM) and n-propyl gallate (PG) from Sigma, as well as the commercial preparation of azoxystrobin Amistar WG (Zeneca Agrochemicals; 50% active ingredient). *N*-Phenylbenzamide derivatives were obtained through the Schötten-Baumann reaction[28–30], with the synthesis of amides from amine derivatives and acyl halides in the presence of aqueous bases. Concentrated stock solutions were prepared in DMSO, except for potassium cyanide, which was dissolved in water and had the pH adjusted to 7 with HCl, and stored at -20 °C. For dose response assays, test compounds were serially diluted in DMSO, such that the final concentration of DMSO was constant across every condition.

2.2. Biological material and growth conditions.

Organisms used were *P. pastoris* X-33 (Invitrogen), *E. coli* BL21 (DE3) Rosetta 2 (Novagen), *M. perniciosa* biotype-S TIR01, *M perniciosa* biotype-C FA553[31], *S. sclerotiorum* and *V. pirina*. *P. pastoris* was grown at 30 °C in YP culture medium (5 g L^{-1} yeast extract and 10 g L^{-1} peptone) with either 3% (v:v) glycerol (YPG) or 1% glycerol (YPG 1%), as indicated throughout the text. *E. coli* was grown in Luria-Broth (5 g L^{-1}

yeast extract, 10 g L^{-1} peptone and 10 g L^{-1} NaCl) and filamentous fungi were cultivated on malt-agar (17 g L^{-1} mat extract, 5 g L^{-1} yeast extract and 2% agar) at 25-28 °C. *M. perniciosa* spores were germinated in LMCpL+ culture medium[32] at 28 °C in the dark.

2.3. *P. pastoris* growth assay and data processing

Freshly streaked *P. pastoris* colonies were inoculated into YPG liquid medium and grown aerobically for 16-24 h at 30 °C. For growth assays in solid YPG, cells were diluted to an optical density of 0.02 (600 nm) or lower, transferred to YPG supplemented with respiration inhibitors (5 mg L^{-1} AZO and 5 mM SHAM) or 1% DMSO and incubated until the appearance of visible colonies. Growth assays in liquid culture medium were performed in 96-well flat-bottomed microtiter plates under agitation, in which 5 mM SHAM or 500 µM NPD were added, as well as DMSO or 0.5 mg L^{-1} AZO. Internal controls were included in each plate, consisting of 1% DMSO and 1% DMSO plus 0.5 mg L^{-1} AZO. Absorbance readings (600 nm) were performed at 15 min intervals (SpectraMax 384, Molecular Devices) for a total of 72 h, and measured values were converted to real values with **Eqn. 1**. OCHT® software was used to fit a sigmoidal curve function of determinate growth[33] and the maximum specific growth rate (µMax) was calculated at the inflection point. Growth parameters obtained from each experiment were normalized as a percentage of the internal controls. For dose-response assays, a four-parameter sigmoid function was fitted (Prism Graphpad, Graphpad Software, Inc.).

$$f(x) = 12.092x^4 - 31.353x^3 + 31.371x^2 - 6.4295x + 0.5974 \quad (1)$$

2.4. Cloning of rMpAOX, site-directed mutagenesis and ectopic expression

The DNA-coding sequence for MpAOX (Genebank ID ABN09948.3) had already been sub-cloned and kindly provided by Paula F. Prado. The region corresponding to the mature protein (e.g., without the 40 amino acid residue N-terminal mitochondrial signaling peptide), as predicted in silico by the Signal P server[34], was amplified by PCR to generate the rMpAOXΔ40 construct. Recognition sites for NdeI and EcoRI restriction enzymes were included to the 5' ends of the PCR primers and used for cloning of the PCR product into the pET28a bacterial expression vector (Novagen) with standard molecular biology procedures. Site-directed mutagenesis of rMpAOXΔ40 was performed with QuikChange II Site-Directed Mutagenesis Kit (Agilent Technologies), and following instructions provided by the manufacturer. Codons coding for threonine 261 and

tyrosine 262 in MpAOX (relative to the full-length protein) were changed to valine and phenylalanine, respectively, based on known inactivating mutations of corresponding residues in *T. brucei* AOX[23]. The ectopic expression of rMpAOXΔ40 in *E. coli* was performed essentially as described elsewhere[25]. *E. coli* cells were transformed with pET28a- rMpAOXΔ40 or the empty vector backbone by electroporation and plated in selective LB medium with 25 µg mL^{-1} kanamycin and 50 µg mL^{-1} chloramphenicol. Individual colonies were picked and inoculated in liquid LB medium with antibiotics and grown at 37 °C and 250 rpm for 16 h. The absorbance at 600 nm was measured (Biochrom WPA CO 8000 Cell Density Meter) and aliquots were transferred to fresh LB medium with antibiotics and 50 µM $FeSO_4$ to a final optical density of 0.01. After 2 h at 30 °C and aeration, expression of the recombinant protein was induced by 25 µM Isopropyl β-D-1-thiogalactopyranoside (IPTG). The culture was kept under the same conditions for another 8 h and cells were harvested and used immediately for oxygen measurement assays.

2.5. Oxygen consumption measurements

Oxygen consumption measurements were performed with a Clark-type oxygen electrode (Oxygraph Plus, Hansatech Instruments). *P. pastoris* was grown on YPG for 16 h and cells were used directly (non-treated), or subjected 5 mg L^{-1} AZO for 4 h to induce the alternative respiration before measurements. *E. coli* expressing rMpAOX was prepared as described. After growth, *P. pastoris* or *E. coli* cells were washed with fresh YPG (glycerol as respiration substrate) and transferred to the oxygraph chamber. The cell concentration was adjusted to give an oxygen consumption rate of ~40 nmol mL^{-1} min^{-1}. Measurements of the alternative respiration were performed in the presence of 2.5 mM KCN. O_2 uptake was recorded before and after addition of DMSO or the test compounds, and the residual respiration was determined as the ratio between the final and initial respiration rates. For dose-response assays, a four-parameter sigmoid function was fitted (Prism Graphpad, Graphpad Software, Inc.).

2.6. Antifungal activity assays

M. perniciosa basidiospores were diluted with LMCpL+ medium to 10^5 mL^{-1} and 100 µL aliquots were transferred to a 96-well plate. NPD 7j-41 or 7j-78 were added into each well, and basidiospore germination and hyphal development were monitored for 21 days. For mycelial growth assays, agar plugs containing active

mycelia from *M. perniciosa*, *S. sclerotiorum* and *V. pirina* were transferred to the center of new culture plates amended with 7j-41 or 7j-78, with or without further addition of 5 mg L^{-1} AZO. Control plates consisted of 0.5% DMSO and 0.5% DMSO plus 5 mg L^{-1} AZO. After 15 days, the mycelial diameter was measured in two orthogonal axes and averaged. For *in planta* assays, 16 day-old seedlings of tomato (*Solanum lycopersicum*) cultivar Micro-Tom (MT) were inoculated with 10^6 basidiospores of *M. perniciosa* S-biotype isolate TIR01 as described elsewhere[35]. 7j-41 at 200 µM or DMSO were mixed with the basidiospore suspension during inoculation, and non-inoculated plants were equally treated. Symptoms were evaluated by measuring the stem diameter[35] at 5, 15, 25 and 35 days after inoculation. The experiment was completely randomized, with 30 plants per treatment, and results were analyzed with Student's t test (R x64 3.4.3).

2.7. PpAOD Molecular modeling and docking

The PpAOD structure was modeled with YASARA[36], using TAO structures with bound ligands as templates (PDB ID 3VVA and 3W54)[23]. Each chain from those structures was individually used as templates. After comparative modeling, the position of the hydroxide ion was optimized in solution through a steep descent and simulated annealing minimization using AMBER14 force field (ff14)[37]. Each PpAOD model was used as input to a molecular docking routine in AutoDock (v. 4.2.5.1)[38] and the best pose of each ligand was obtained after 5 runs. Model performance was evaluated through the BEDROC metric[39], by comparing their biological activity and docking scores. For this purpose, the 30 PpAOD-selective NPD were ranked and the first quartile (8 compounds) was defined as active, whereas the rest was considered inactive. The BEDROC function was implemented in MatLab R2011a (Mathworks) with alpha values of 6 and 20. The cavity volume was generated with KVFinder[40].

3. Results

3.1. Pichia pastoris as a fungal model for AOX inhibitor characterization

It has been previously shown that *P. pastoris* possesses a functional AOX (PpAOD), although not constitutively expressed[41]. Here, we demonstrate that PpAOD is induced by the fungicide and ETC inhibitor azoxystrobin (AZO), which shifts the O_2 uptake from a cyanide-sensitive (main respiration) to a cyanide-insensitive (alternative respiration) pathway. Accordingly, classic AOX inhibitors SHAM and n-propyl gallate

blocked the alternative respiration and demonstrate that AOX allows oxygen consumption to continue in the presence of AZO **(Fig 1A)**. PpAOD also contributes to *P. pastoris* growth on AZO, albeit at a lower speed, and only the combination of AZO and SHAM abolished the formation of visible colonies **(Fig 1B)**.

P. pastoris grows to high cell densities in liquid culture, which interferes with automated absorbance readings. To avoid this problem, the glycerol concentration in YP medium was reduced to 1% to limit cell growth. Furthermore, a standard curve with known *P. pastoris* cell densities was generated and used to determine the correct absorbance of unknown samples. The maximal specific growth rate (µMax) in liquid culture medium was thus determined and provided an accurate estimate of *P. pastoris* growth capacity before and after the inhibition of cellular respiration **(S1 Fig)**.

Next, AZO-treated *P. pastoris* was employed to functionally characterize 74 *N*-Phenylbenzamide derivatives (NPD) synthesized by our group in search of novel fungal AOX inhibitors. DMSO-treated *P. pastoris* was used as a control to evaluate the selectivity of those compounds with respect to the alternative respiration **(Fig 2)**. At 500 µM, the tested NPD exerted little effect upon the main respiration, with an average inhibition of 8 ± 9% in O_2 uptake and 13 ± 21% of growth rate. On the other hand, the alternative respiration was inhibited by 65 ± 21%, and the PpAOD-driven growth by 40 ± 29%. There was a marked difference in activity of some NPD after comparison of respiration and growth measurements, such as 7j-07, 7j-25, 7j-42 and 7j-91 to name a few. This suggests that 1) toxic/unspecific compounds active only in growth assays may have off-targets other than ETC components; and 2) the cellular environment greatly influences the biological effect of NPD, possibly due to the cellular metabolism of xenobiotics. For instance, some AOX-targeting NPD did not reduce cell growth, which might be explained by cytochrome P450 metabolism or detoxification through efflux pumps, two known mechanisms of drug resistance in fungi[42,43].

Overall, 69 of the 74 tested NPD led to statistically significant inhibition of the alternative respiration. However, 42 of those 74 also interfered either with the O_2 uptake or with the cellular growth in control conditions (without AZO). Of the 31 NPD exclusively active after AZO treatment, 12 affected the alternative respiration and not the cellular growth; one reduced cellular growth and not the alternative respiration; and 16 NPD selectively inhibited both the alternative respiration and cellular growth. Only one NPD, 7j-78, had no

appreciable effect in any circumstance. This data is fully available in **S1 Table** and at PubChem bioassay database (PubChem AID: 1259412).

From the set of selective PpAOD inhibitors active both in O_2 uptake and cellular growth, 7j-41 was the most potent *P. pastoris* growth inhibitor. Therefore, 7j-41 was selected for further characterization and compared with SHAM. Both compounds displayed similar IC_{50} values on *P. pastoris* alternative respiration (208.9 µM and 261.8 µM, respectively) **(Fig 3A),** but 7j-41 was remarkably a more potent growth inhibitor than SHAM (respective IC_{50} of 40.7 µM and 367.6 µM; **Fig 3B**). In order to evaluate those compounds on a different fungal AOX, the recombinant *M. perniciosa* AOX (rMpAOX) was expressed in *E. coli* and O_2 consumption was measured. Indeed, rMpAOX expression created a cyanide-insensitive respiration in *E. coli*, which was not seen either in the negative control (empty vector backbone) or after the expression of mutated rMpAOX versions containing known inactivating amino acid substitutions[23] **(S2 Fig)**. The IC_{50} of 7J-41 on rMpAOX was 178.9 µM, comparable to PpAOD. Conversely, rMpAOX was less responsive to SHAM, which inhibited only 20% of the cyanide-insensitive O_2 uptake at 2.5 mM. At 10 mM SHAM, 60% inhibition was achieved; however, off-target effects of the same magnitude were seen on *E. coli* main respiration **(Fig 3C)**. Thus, we have shown that 7j-41 possess better activity than SHAM on *P. pastoris* growth and on rMpAOX.

3.2. NPD 7j-41 displays antifungal activity against filamentous fungal phytopathogens

The next step was to assess the antifungal activity of 7J-41 against filamentous fungi. We selected three phytopathogens for which AOX is involved in resistance to ETC inhibitors. *M. perniciosa* and *S. sclerotiorum* have been described elsewhere[3,16], and we demonstrate here that the same phenomenon occurs in *V. pirina*. A BlastP search performed against the *V. pirina* genome[44] in JGI Mycocosm Portal and MpAOX as query returned one AOX-coding sequence. Namely, Protein Model 209839 in Scaffold 14 with 57.4% identity. It was also seen that *V. pirina* is able to grow on AZO, but not in the combination of AZO and SHAM **(S3 Fig)**. Hence, we investigated the effect of 7j-41 alone or with AZO on the mycelial development of the three selected phytopathogens. NPD 7j-78 **(Fig 4A)**, which did not display any activity on *P. pastoris* was evaluated as well. As shown in **Fig 4B**, a combination of AZO and 500 µM 7j-41 reduced the *in vitro* radial growth of *M. perniciosa*, *S. sclerotiorum* and *V. pirina*, when compared to AZO alone. Remarkably, *V. pirina* was sensitive to SHAM and 7J-41 alone, in the absence of AZO **(Fig 4B and S3 Fig)**.

During the witches' broom disease of cocoa, MpAOX is highly expressed in early developmental stages of *M. perniciosa*, and the biotrophic-like mycelium is sensitive to SHAM *in vitro* even in the absence of AZO[3]. In agreement, we observed a complete inhibition of *M. perniciosa* basidiospore germination with 125 µM 7j-41, while the inert 7j-78 did not exert any effect up to the maximal tested concentration of 250 µM **(Fig 4C)**. For comparison, SHAM abolished *M. perniciosa* basidiospore germination only at 5 mM **(S4 Fig)**, which is the same concentration used previously in *in vitro* mycelial growth assays[3].

Finally, the antifungal activity of 7j-41 was evaluated *in planta* against *M. perniciosa* **(Fig 5)**. We observed that 200 µM 7j-41 completely prevented WBD symptom appearance in infected tomato (*Solanum lycopersicum*) plants, which usually consist of stem swelling, axillary shoot growth and leaf distortion[35]. Even 35 days after inoculation, no difference was seen in stem diameter between non-inoculated plants and inoculated, 7j-41-treated plants **(Fig. 4D)**. 7j-41 did not exert appreciable effects on non-inoculated control plants. Here, we demonstrated that 7j-41 is active against filamentous fungi that are threats to crops worldwide, including *M. perniciosa*, for which there is currently no chemical treatment available.

3.3. A PpAOD structural model provides insights on NPD structure-activity relationships

In order enlighten the NPD structure-activity relationship and gain insights for the development of antifungal agents based on AOX inhibition, we compared the NPD biological activity on *P. pastoris* and their modeled interactions with PpAOD. Initially we generated 21 distinct PpAOD structural models based on TAO (46.2% sequence identity). We selected as templates TAO structures bound with the ascofuranone derivative AF2779OH (PDB ID: 3VVA) and with colletochlorin B (PDB ID: 3W54)[23]. The apo TAO structure (PDB ID: 3VV9) was not used because the volume of the binding site is smaller than the NPD. Subsequently, 30 NPD that were selective inhibitors of *P. pastoris* alternative respiration were docked into each PpAOD structural model. Model performance was evaluated with the BEDROC metric and two distinct α values[39] **(S5 Fig)**, and the PpAOD model that generated the highest correlation with experimental data was selected for investigation **(Fig 6)**. Thus, NPD structure-activity relationships and protein-ligand interactions are discussed below.

PpAOD inhibitors show a clear preference for polarizable and bulkier halogen atoms from higher periods, such as Cl, Br and I. Their greater volumes allow for more points of contact, which leads to a higher

affinity to the PpAOD active site. Moreover, NPD with F and Cl substitutions were more effective growth inhibitors, which is explained by the fact that such atoms may prevent drug degradation by the cellular metabolism[45]. In general, the *meta* position of the aromatic ring bonded to the amide nitrogen atom favors electronegative substituents for better antifungal activity.

Substituents R_1 and R_2 **(S1 Table)** define which of the two benzene rings will be positioned more internally with respect to PpAOD active site. F, Cl and I favor the insertion of their benzene ring to which they are attached, which is due to their interaction with the region corresponding to Phe134, Leu137, Glu138 and Tyr235. These resides are in the vicinity of the PpAOD diiron center, and the hydroxide radical bridging the two iron atoms may also interact with *meta* substituents in some NPD. The NPD carbonil group is usually directed towards Arg97 and an electrostatic interaction is predicted, although the geometry of this interaction does not permit the establishment of a hydrogen bond. The nitrogen atom of the NPD amide interacts with PpAOD α-helix 5 - following TAO's structure nomenclature[23] -, and it is possible for a hydrogen bond to occur between that nitrogen and Glu230 backbone carbonyl group.

Van der Walls forces also play an important role in protein-ligand interaction. A π stacking interaction occurs between benzene rings from NPD and Phe100, which are positioned orthogonally with respect to each other. Additionally, we observed ligand interactions with Met93, Arg97, Trp130, Arg133 and Thr234. R2 substituents, when directed towards the outside of the active site, are positioned according to their size. For instance, F atoms interact with a small hydrophobic cavity formed by Met93, Leu227 and C_β and C_γ of Glu230. Bulkier atoms, such as Cl, Br and I, do no interact with that small hydrophobic cavity and are instead directed towards the entrance of the active site. NPD with poor biological activity and low docking scores usually exhibit polar substituents in close proximity to hydrophobic regions, or fewer points of interaction due to small substituents, such as hydrogen **(S6 Fig)**.

In their most stable conformation, NPD present a delocalized π electronic system. However, the ligand's aromatic rings are reoriented when inside PpAOD active site, in order to favor the protein-ligand interaction. Substituents that intensify the electronic delocalization, such as NO_2, disfavor that rearrangement and, therefore,

are weak ligands. Furthermore, NO_2 is a polar group that interacts weakly with hydrophobic residues in the active site.

4. Discussion

AOX is a desirable target for the development of new antiparasitic and antifungal agents, with clear potential impacts on human health and food security, since AOX inhibitors might be used to treat human fungal pathogens[46–49], as well as phytopathogens[3,14–17]. Here, we presented the first comprehensive study on fungal AOX inhibition by small molecules and provide new tools to aid the development of novel fungicides.

Here, the yeast *Pichia pastoris* was employed as a fungal model to assess the antifungal potential of those compounds. Usually, *Saccharomyces cerevisiae* is used as a host for heterologous expression of fungal AOXs because it lacks its own AOX[50–52]. However, our experience shows that *S. cerevisiae* was not a robust model for testing AOX-driven growth (data not shown), and we reason that it is because *S. cerevisiae* lacks a functional ETC complex I, the only ETC component that contributes to ATP synthesis when AOX is the sole terminal oxidase. The AOX-expressing *P. pastoris*, on the other hand, can readily grow on a non-fermentable carbon source, such as glycerol, using complex I to generate ATP. This allowed us to functionally characterize our NPD library and identify the selective PpAOD inhibitor 7j-41. Overall, 7j-41 was more potent than SHAM as an antifungal agent and was effective against three non-model filamentous fungi that are threats to crops worldwide, *M. perniciosa*, *S. sclerotiorum* and *V. pirina*. Finally, an experimentally validated structural model of PpAOD was generated, which provided useful information on protein-ligand interactions and NPD structure-activity relationship.

M. perniciosa was the first phytopathogen for which compelling evidence has been obtained on the relevance of AOX during host infection. Throughout *M. perniciosa* life cycle, MpAOX is overexpressed in biotrophic phase, when the living cocoa produces large amounts of the potent ETC inhibitor nitric oxide. Indeed, parallels were drawn between *M. perniciosa* and the human parasite *T. brucei* with respect to the dependence on the alternative respiration for virulence and survival[3]. Here, we demonstrated that AOX inhibitor 7j-41 alone was enough to prevent *M. perniciosa in vitro* spore germination and abolished the appearance of WBD symptoms in

infected plants. Notably, SHAM has been shown to prevent *M. grisea* and *Botrytis cinerea* spore germination *in vitro*[53,54], suggesting that AOX activity is a common feature needed for spore germination in these fungi.

On the other hand, disease development is not always dependent on AOX, since *M. grisea* AOX knock-out strains displayed similar virulence levels in barley leaves as did the wild-type[13]. However, the relevance of fungal AOX in agricultural settings is also related to AOX's contribution to fungicide resistance. Strobilurins are quinone outside (complex III) inhibitors successfully employed as agrochemicals for more than 20 years[55], and the escape mechanism through the alternative respiration has been thoroughly discussed and exemplified[11,19]. Moreover, the non-ETC targeting fungicide procymidone has been shown to induce AOX expression in *S. sclerotiorum*[16]; and C*andida albicans* AOX provides resistance against azole fungicides[12,56]. This is in accordance with studies on yeasts demonstrating that mitochondrial function as a whole plays a great part in fungal virulence and resistance to antifungal agents[57]. Collectively, those results indicate that AOX plays a broader role in fungal development and expands the scenarios in which AOX-targeting molecules can be effectively employed to treat fungal diseases (i.e., in combination with other AOX-inducing molecules).

Overall, our data demonstrate that 7j-41 is more potent and selective than SHAM against *M. perniciosa*, which is evidenced by the difference in concentrations used (10-20 times higher for SHAM than 7j-41) and by non-specific effects in *E. coli* membranes with SHAM. We envisage that our results and the uncovered NPD structure-activity relationship will guide AOX-targeting fungicide development against *M. perniciosa* and other fungal threats to crops worldwide.

5. Acknowledgements

This work was supported by The São Paulo Research Foundation (FAPESP) through research grants 2015/07653-5 and 2016/10498-4, and scholarships 2014/15339-6, 2015/09870-3, 2015/06677-8 and 2017/17000-4. This work was also supported by the National Council for Scientific and Technological Development (CNPq) grant 475535/2013-8 and scholarship 142358/2014-2. The authors also acknowledge the Brazilian Biosciences National Laboratory (LNBio-CNPEM/MCTI), specifically the Nuclear Magnetic Resonance and Chemistry and Natural Products Laboratories. The authors thank Rafael Guido for his valuable support on the rational design studies.

6. Author contribution

Wrote the manuscript: M.R.O.B., J.G.C.P., P.C.S.C., S.A.R.; NPD synthesis and structural characterization: M.L.V., J.S., F.H.S.R., M.L.S., S.A.R.; *P. pastoris* and antifungal assays *in vitro*: M.R.O.B., B.A.P., A.C., F.M., A.T.C., M.F.C., G.A.G.P.; *in planta* assays: S.E.M., D.P., A.F.; structural modeling and structure activity-relationship determination: J.G.C.P., P.C.S.C., P.C.M.L.M., P.S.L.O., M.F.C.; Conceptualization: G.A.G.P.

7. References

1 Meinhardt LW, Rincones J, Bailey BA, Aime MC, Griffith GW, Zhang D, *et al.*, Moniliophthora perniciosa, the causal agent of witches' broom disease of cacao: what's new from this old foe?, Mol Plant Pathol **9**:577–588 (2008).

2 Teixeira PJPL, Thomazella DP de T, and Pereira GAG, Time for Chocolate: Current Understanding and New Perspectives on Cacao Witches??? Broom Disease Research, PLoS Pathog **11**:1–8 (2015).

3 Thomazella DPT, Teixeira PJPL, Oliveira HC, Saviani EE, Rincones J, Toni IM, *et al.*, The hemibiotrophic cacao pathogen Moniliophthora perniciosa depends on a mitochondrial alternative oxidase for biotrophic development., New Phytol **194**:1025–1034 (2012).

4 Teixeira PJPL, Thomazella DPDTDT, Reis O, do Prado PFV, do Rio MCS, Fiorin GL, *et al.*, High-Resolution Transcript Profiling of the Atypical Biotrophic Interaction between Theobroma cacao and the Fungal Pathogen Moniliophthora perniciosa, Plant Cell **26**:4245–4269 (2014).

5 McDonald AE and Vanlerberghe GC, Origins, evolutionary history, and taxonomic distribution of alternative oxidase and plastoquinol terminal oxidase, Comp Biochem Physiol Part D Genomics Proteomics **1**:357–364 (2006).

6 McDonald AE, Alternative oxidase: What information can protein sequence comparisons give us?, Physiol Plant **137**:328–341 (2009).

7 Rogov AG, Sukhanova EI, Uralskaya LA, Aliverdieva DA, and Zvyagilskaya RA, Alternative oxidase: Distribution, induction, properties, structure, regulation, and functions, Biochem **79**:1615–1634 (2014).

8 Gupta KJ, Mur LAJ, and Neelwarne B, eds., Alternative respiratory pathways in higher plants, John Wiley & Sons, Ltd, Chichester, UK (2015).

9 Taiz L and Zeiger E, Respiration and Lipid metabolism, ed. by Taiz L and Zeiger E, Plant Physiology and Development, Sinauer Associates, Sunderland, pp. 223–258 (2003).

10 Del-Saz NF, Ribas-Carbo M, McDonald AE, Lambers H, Fernie AR, and Florez-Sarasa I, An In Vivo Perspective of the Role(s) of the Alternative Oxidase Pathway, Trends Plant Sci **23** (2017).

11 Fernández-Ortuño D, Torés JA, de Vicente A, and Pérez-García A, Mechanisms of resistance to QoI fungicides in phytopathogenic fungi., Int Microbiol **11**:1–9 (2008).

12 Yan L, Li M, Cao Y, Gao P, Cao Y, Wang Y, *et al.*, The alternative oxidase of Candida albicans causes reduced fluconazole susceptibility, J Antimicrob Chemother **64**:764–773 (2009).

13 Avila-Adame C and Köller W, Disruption of the alternative oxidase gene in Magnaporthe grisea and its impact on host infection., Mol Plant Microbe Interact **15**:493–500 (2002).

14 Affourtit C, Heaney SP, and Moore AL, Mitochondrial electron transfer in the wheat pathogenic fungus Septoria tritici: on the role of alternative respiratory enzymes in fungicide resistance, Biochim Biophys Acta - Bioenerg **1459**:291–298 (2000).

15 Miguez M, Reeve C, Wood PM, and Hollomon DW, Alternative oxidase reduces the sensitivity of Mycosphaerella graminicola to QOI fungicides, Pest Manag Sci **60**:3–7 (2004).

16 Xu T, Wang Y-T, Liang W-S, Yao F, Li Y-H, Li D-R, *et al.*, Involvement of alternative oxidase in the regulation of sensitivity of Sclerotinia sclerotiorum to the fungicides azoxystrobin and procymidone, J Microbiol **51**:352–358 (2013).

17 Olaya G, Zheng D, and Köller W, Differential responses of germinating Venturia inaequalis conidia to kresoxim-methyl, Pestic Sci **54**:230–236 (1998).

18 Joseph-Horne T, Wood PM, Wood CK, Moore AL, Headrick J, and Hollomon D, Characterization of a split respiratory pathway in the wheat 'take-all' fungus, Gaeumannomyces graminis var. tritici, J Biol Chem **273**:11127–11133 (1998).

19 Wood PM and Hollomon DW, A critical evaluation of the role of alternative oxidase in the performance of strobilurin and related fungicides acting at the Qo site of complex III., Pest Manag Sci **59**:499–511 (2003).

20 Walker AS, Auclair C, Gredt M, and Leroux P, First occurrence of resistance to strobilurin fungicides in Microdochium nivale and Microdochium majus from French naturally infected wheat grains, Pest Manag Sci **65**:906–915 (2009).

21 Hayashi K, Watanabe M, Tanaka T, and Uesugi Y, Cyanide-insensitive Respiration of Phytopathogenic Fungi Demonstrated by Antifungal Joint Action of Respiration Inhibitors, J Pestic Sci **21**:399–403 (1996).

22 Menzies SK, Tulloch LB, Florence GJ, and Smith TK, The trypanosome alternative oxidase: a potential drug target?, Parasitology **145**:175–183 (2018).

23 Shiba T, Kido Y, Sakamoto K, Inaoka DK, Tsuge C, Tatsumi R, *et al.*, Structure of the trypanosome cyanide-insensitive alternative oxidase, Proc Natl Acad Sci **110**:4580–4585 (2013).

24 May B, Young L, and Moore AL, Structural insights into the alternative oxidases: are all oxidases made equal?, Biochem Soc Trans **45**:731–740 (2017).

25 Saimoto H, Kido Y, Haga Y, Sakamoto K, and Kita K, Pharmacophore identification of ascofuranone, potent inhibitor of cyanide-insensitive alternative oxidase of Trypanosoma brucei, J Biochem **153**:267–273 (2013).

26 West RA, O'Doherty OG, Askwith T, Atack J, Beswick P, Laverick J, *et al.*, African trypanosomiasis:

Synthesis & SAR enabling novel drug discovery of ubiquinol mimics for trypanosome alternative oxidase, Eur J Med Chem **141**:676–689, Elsevier Masson SAS (2017).

27 Ebiloma GU, Ayuga TD, Balogun EO, Gil LA, Donachie A, Kaiser M, *et al.*, Inhibition of trypanosome alternative oxidase without its N-terminal mitochondrial targeting signal (ΔMTS-TAO) by cationic and non-cationic 4-hydroxybenzoate and 4-alkoxybenzaldehyde derivatives active against T. brucei and T. congolense, Eur J Med Chem **150**:385–402, Elsevier Masson SAS (2018).

28 Baumann E, Ueber eine einfache Methode der Darstellung von Benzoësäureäthern, Berichte der Dtsch Chem Gesellschaft **19**:3218–3222 (1886).

29 Schotten C, Ueber die Oxydation des Piperidins, Berichte der Dtsch Chem Gesellschaft **17**:2544–2547 (1884).

30 Kurti L and Czako B, Strategic Applications of Named Reactions in Organic Synthesis, 1sted., Elsevier Academic Press, San Diego, CA (2005).

31 Mondego JMC, Carazzolle MF, Costa GGL, Formighieri EF, Parizzi LP, Rincones J, *et al.*, A genome survey of Moniliophthora perniciosa gives new insights into Witches' Broom Disease of cacao., BMC Genomics **9**:548 (2008).

32 Meinhardt LW, Bellato CDM, Rincones J, Azevedo RA, Cascardo JCM, and Pereira GAG, In vitro production of biotrophic-like cultures of Crinipellis perniciosa, the causal agent of witches' broom disease of Theobroma cacao., Curr Microbiol **52**:191–196 (2006).

33 Yin X, A Flexible Sigmoid Function of Determinate Growth, Ann Bot **91**:361–371 (2003).

34 Petersen TN, Brunak S, von Heijne G, and Nielsen H, SignalP 4.0: discriminating signal peptides from transmembrane regions., Nat Methods **8**:785–786 (2011).

35 Deganello J, Leal GA, Rocha ML, Peres LEP, and Figueira A, Interaction of moniliophthora perniciosa biotypes with micro-tom tomato: A model system to investigate the witches' broom disease of theobroma

cacao, Plant Pathol:1–13 (2014).

36 Krieger E, Joo K, Lee J, Lee J, Raman S, Thompson J, *et al.*, Improving physical realism, stereochemistry, and side-chain accuracy in homology modeling: Four approaches that performed well in CASP8, Proteins Struct Funct Bioinforma **77**:114–122 (2009).

37 Maier JA, Martinez C, Kasavajhala K, Wickstrom L, Hauser KE, and Simmerling C, ff14SB: Improving the Accuracy of Protein Side Chain and Backbone Parameters from ff99SB, J Chem Theory Comput **11**:3696–3713 (2015).

38 Morris GM, Huey R, Lindstrom W, Sanner MF, Belew RK, Goodsell DS, *et al.*, AutoDock4 and AutoDockTools4: Automated docking with selective receptor flexibility, J Comput Chem **30**:2785–2791 (2009).

39 Truchon J-F and Bayly CI, Evaluating Virtual Screening Methods: Good and Bad Metrics for the "Early Recognition" Problem, J Chem Inf Model **47**:488–508 (2007).

40 Oliveira SH, Ferraz FA, Honorato R V, Xavier-Neto J, Sobreira TJ, and de Oliveira PS, KVFinder: steered identification of protein cavities as a PyMOL plugin, BMC Bioinformatics **15**:197 (2014).

41 Kern A, Hartner FS, Freigassner M, Spielhofer J, Rumpf C, Leitner L, *et al.*, Pichia pastoris 'just in time' alternative respiration, Microbiology **153**:1250–1260 (2007).

42 Anderson JB, Evolution of antifungal-drug resistance: mechanisms and pathogen fitness., Nat Rev Microbiol **3**:547–556 (2005).

43 Shin J, Kim J-E, Lee Y-W, and Son H, Fungal Cytochrome P450s and the P450 Complement (CYPome) of Fusarium graminearum, Toxins (Basel) **10**:112 (2018).

44 Cooke IR, Jones D, Bowen JK, Deng C, Faou P, Hall NE, *et al.*, Proteogenomic Analysis of the Venturia pirina (Pear Scab Fungus) Secretome Reveals Potential Effectors, J Proteome Res **13**:3635–3644 (2014).

45 Murphy CD and Sandford G, Recent advances in fluorination techniques and their anticipated impact on drug metabolism and toxicity, Expert Opin Drug Metab Toxicol **11**:589–599 (2015).

46 Martins VP, Dinamarco TM, Soriani FM, Tudella VG, Oliveira SC, Goldman GH, *et al.*, Involvement of an Alternative Oxidase in Oxidative Stress and Mycelium-to-Yeast Differentiation in Paracoccidioides brasiliensis, Eukaryot Cell **10**:237–248 (2011).

47 Guedouari H, Gergondey R, Bourdais A, Vanparis O, Bulteau AL, Camadro JM, *et al.*, Changes in glutathione-dependent redox status and mitochondrial energetic strategies are part of the adaptive response during the filamentation process in Candida albicans, Biochim Biophys Acta - Mol Basis Dis **1842**:1855–1869, Elsevier B.V. (2014).

48 Magnani T, Soriani FM, Martins VDP, Policarpo ACDF, Sorgi CA, Faccioli LH, *et al.*, Silencing of mitochondrial alternative oxidase gene of Aspergillus fumigatus enhances reactive oxygen species production and killing of the fungus by macrophages, J Bioenerg Biomembr **40**:631–636 (2008).

49 Akhter S, McDade HC, Gorlach JM, Heinrich G, Cox GM, and Perfect JR, Role of Alternative Oxidase Gene in Pathogenesis of Cryptococcus neoformans, Infect Immun **71**:5794–5802 (2003).

50 Magnani T, Soriani FM, Martins VP, Nascimento AM, Tudella VG, Curti C, *et al.*, Cloning and functional expression of the mitochondrial alternative oxidase of Aspergillus fumigatus and its induction by oxidative stress, FEMS Microbiol Lett **271**:230–238 (2007).

51 Huh W-K and Kang S-O, Characterization of the gene family encoding alternative oxidase from Candida albicans, Biochem J **356**:595–604 (2001).

52 Robertson A, Schaltz K, Neimanis K, Staples JF, and McDonald AE, Heterologous expression of the Crassostrea gigas (Pacific oyster) alternative oxidase in the yeast Saccharomyces cerevisiae, J Bioenerg Biomembr **48**:509–520, Journal of Bioenergetics and Biomembranes (2016).

53 Avila-Adame C and Köller W, Impact of alternative respiration and target-site mutations on responses of

germinating conidia of Magnaporthe grisea to Qo-inhibiting fungicides, Pest Manag Sci **59**:303–309 (2003).

54 Inoue K, Tsurumi T, Ishii H, Park P, and Ikeda K, Cytological evaluation of the effect of azoxystrobin and alternative oxidase inhibitors in Botrytis cinerea, FEMS Microbiol Lett **326**:83–90 (2012).

55 Bartlett DW, Clough JM, Godwin JR, Hall AA, Hamer M, and Parr-Dobrzanski B, The strobilurin fungicides., Pest Manag Sci **58**:649–662 (2002).

56 Strippoli V, D'Auria FD, Tecca M, Callari A, and Simonetti G, Propyl gallate increases in vitro antifungal imidazole activity against Candida albicans, Int J Antimicrob Agents **16**:73–76 (2000).

57 Shingu-Vazquez M and Traven A, Mitochondria and Fungal Pathogenesis: Drug Tolerance, Virulence, and Potential for Antifungal Therapy, Eukaryot Cell **10**:1376–1383 (2011).

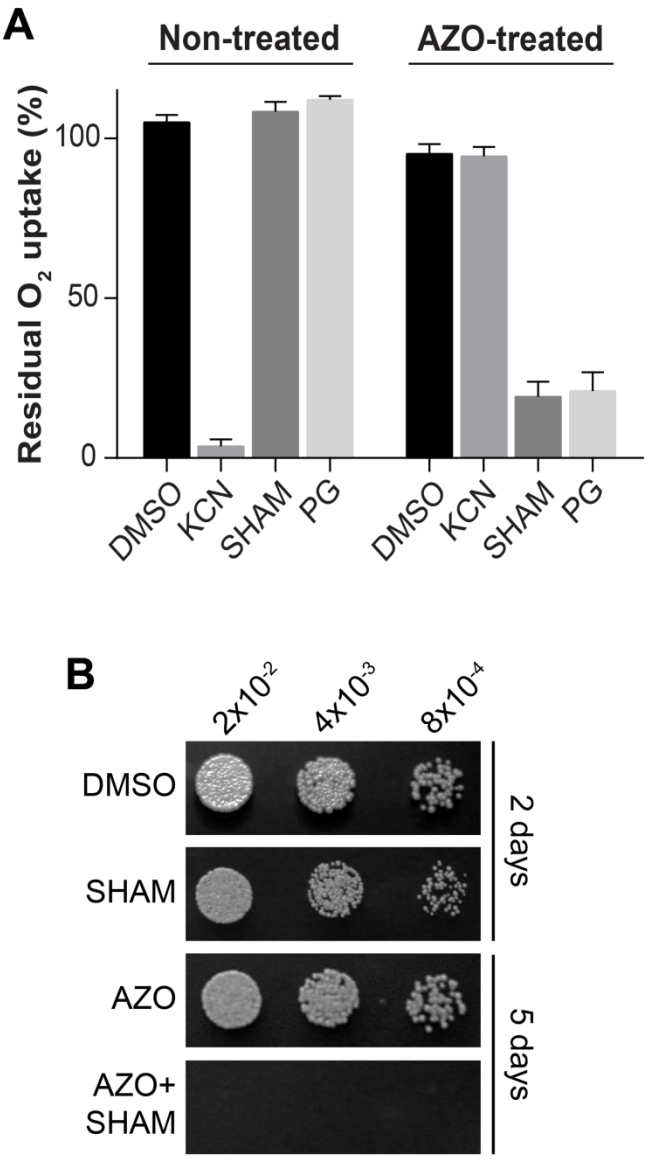

Fig 1. P. pastoris alternative respiration and growth. (A) Azoxystrobin induces the alternative respiration in P. pastoris. P. pastoris was treated (AZO-treated) for 4h with 5 mg L-1 AZO or not (non-treated) before each measurement. Bars depict mean ± SD (n = 3) KCN: 2.5 mM potassium cyanide (main respiration inhibitor); SHAM and PG: 5 mM salicylhydroxamic acid and 1 mM n-propyl gallate (AOX inhibitors). (B) P. pastoris growth in solid culture medium. P. pastoris cells from a pre-culture were transferred to YPG medium amended with 5 mg L-1 AZO, 5 mM SHAM or both. Cell density is indicated on top. The alternative respiration sustains P. pastoris growth on AZO, albeit at a slower rate, and AZO plus SHAM abolished cellular growth.

107x200mm (600 x 600 DPI)

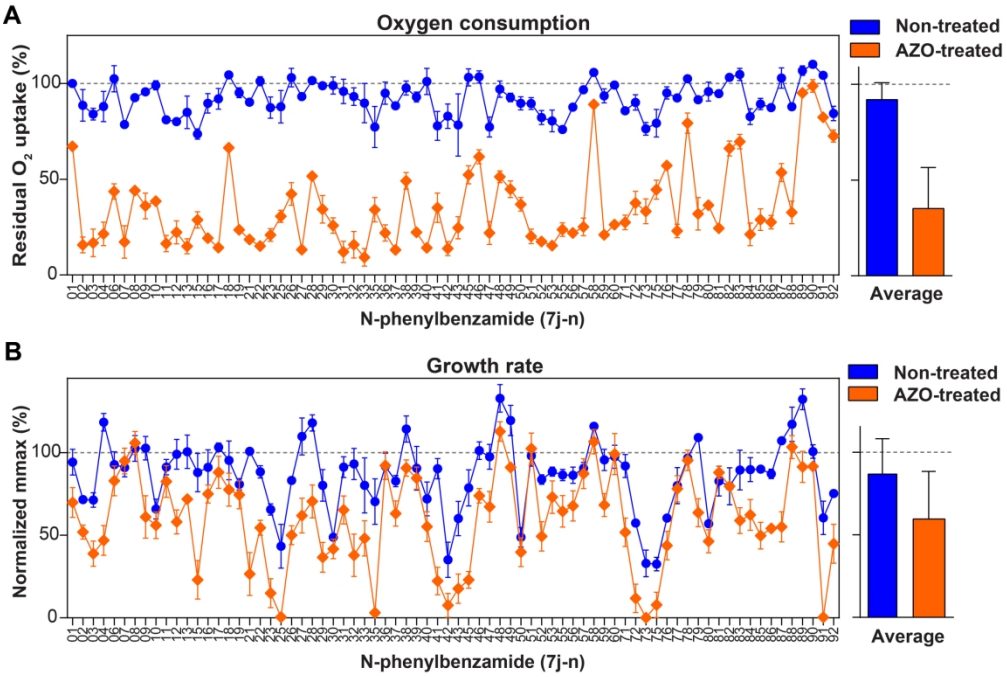

Fig 2. N-Phenylbenzamide functional characterization. (A) Effect on oxygen consumption rate of each tested NPD (left; mean ± SEM) and mean ± SD of all measurements (right). Main respiration: blue symbols; alternative respiration: orange symbols (B) Maximal growth rates in liquid culture medium sustained by the main (non-treated) and the alternative respiration (AZO-treated) in the presence of each NPD (left; mean ± SEM) mean ± SD of all values (right). Full data is presented in S1 Table.

102x69mm (600 x 600 DPI)

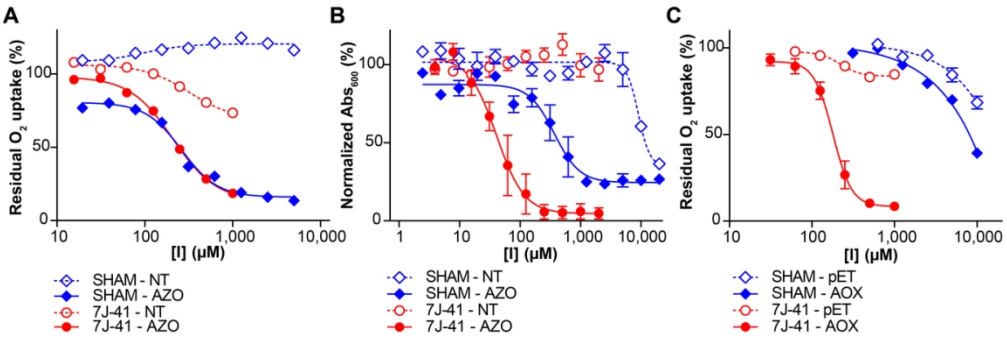

Fig 3. Dose-response assays with SHAM and 7j-41. (A) P. pastoris O2 uptake after addition of SHAM or NPD 7j-41 at varying concentrations, before (NT) or after (AZO) treatment. (B) Relative growth of P. pastoris in liquid culture medium, as measured by the final optical density after 72 h of growth, normalized by the control condition (not treated). (C) O2 uptake of whole E. coli cells transformed with rMpAOXΔ40 (AOX) or the pET28 empty backbone (pET).

58x19mm (600 x 600 DPI)

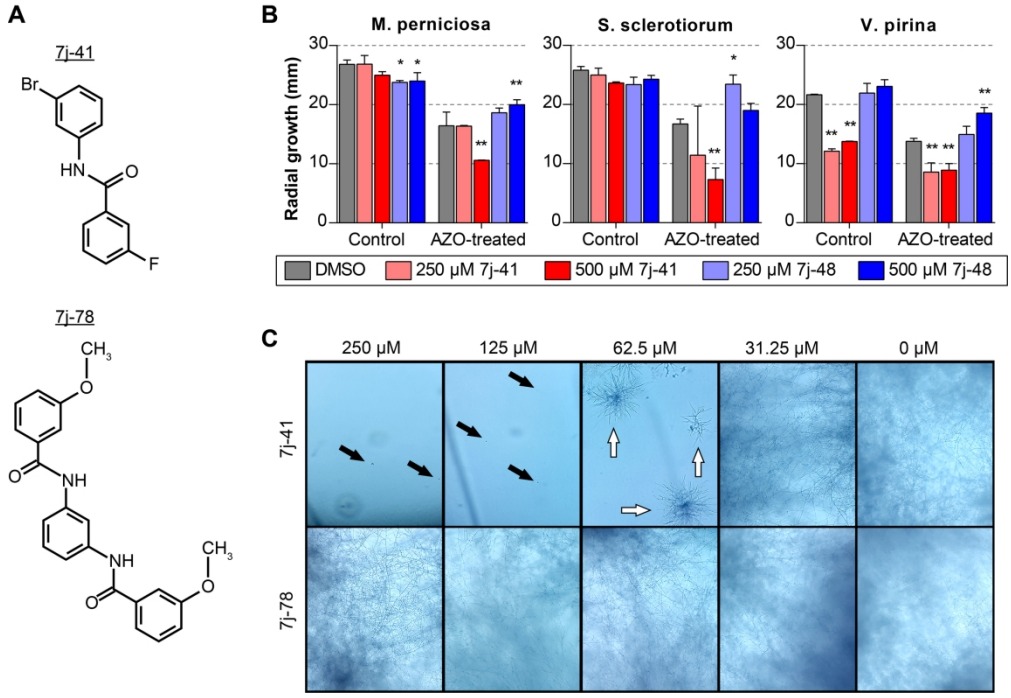

Fig 4. In vitro antifungal activity of NPD 7j-41. (A) Phytopathogens M. perniciosa, S. sclerotiorum and V. pirina were grown with the active NPD 7j-41 and the inert NPD 7j-78, with or without further addition of 5 mg L-1 AZO. Bars depict the radial growth of the mycelia (mean ± SD; n = 3). Asterisks indicate results statistically different from DMSO treatment (with or without AZO, as pertinent). *: $p < 0.05$; **: $p < 0.01$. For the three tested fungal species, 500 µM 7j-41 increased their sensitivity to AZO. Notably, V. pirina is sensitive to 7j-41 even in the absence of AZO. (B) M. perniciosa basidiospores germination assay. After 21 days, fully developed mycelium was observed in every condition with 7j-78, whereas 7j-41 exhibited inhibitory effects on spore germination from 62.5 µM. Black arrows: non-germinated spores. White arrows: partially developed mycelium.

110x76mm (600 x 600 DPI)

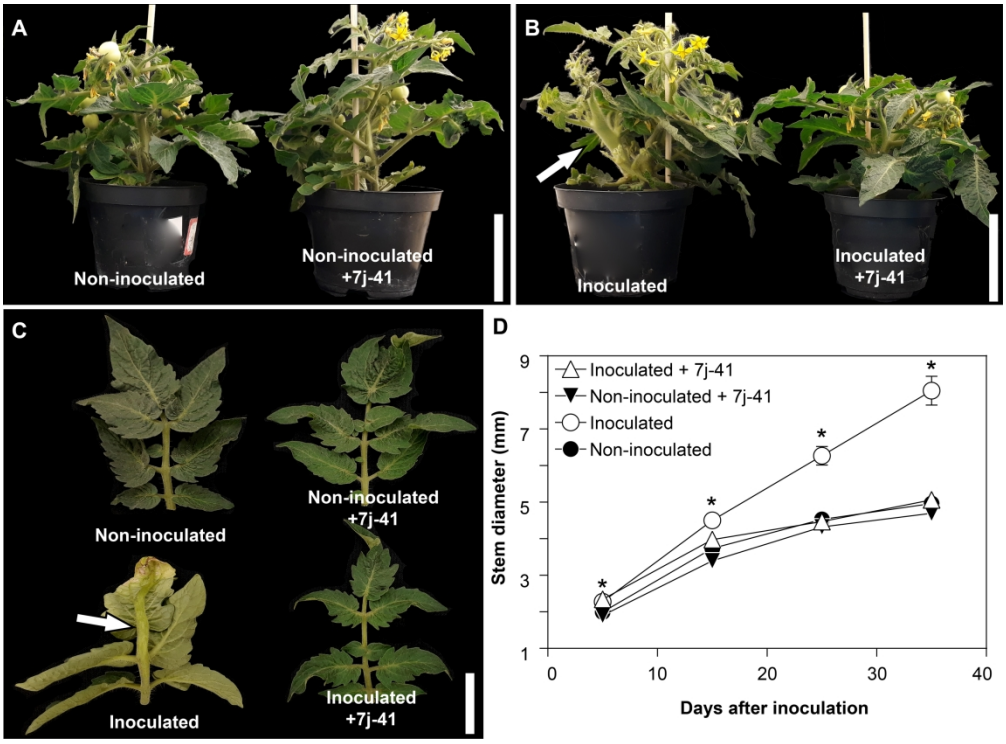

Fig 5. In planta antifungal activity of NPD 7j-41 against M. perniciosa. MT plants 35 days after inoculation with spores from S-biotype isolate of M. perniciosa were compared with the controls treatment. (A) At left, Non-inoculated MT (treated only with DMSO) and at right, non-inoculated MT treated with 7j-41 displaying no differences between them (controls). (B) At left, MT inoculated with M. perniciosa displaying stem swelling and the arrow shows the abnormal axillary outgrowth (broom), and at right, plant inoculated together with 7j-41 displaying no symptoms. (C) MT leaves inoculated with M. perniciosa displaying petiole swelling compared with the other treatments which present no symptoms. (D) Mean of stem diameter from MT inoculated with M. perniciosa biotype-S, non-inoculated, inoculated with M. perniciosa, treated with 7j41 molecule and non-inoculated treated with 7j41 molecule at 5, 15, 25 and 35 days after inoculation. (Average ± SD; n=30). Asterisks indicate results statistically different from the non-inoculated control. *: $p<0.05$. Scale Bar: 6 cm (a, b), 2 cm (c).

129x94mm (600 x 600 DPI)

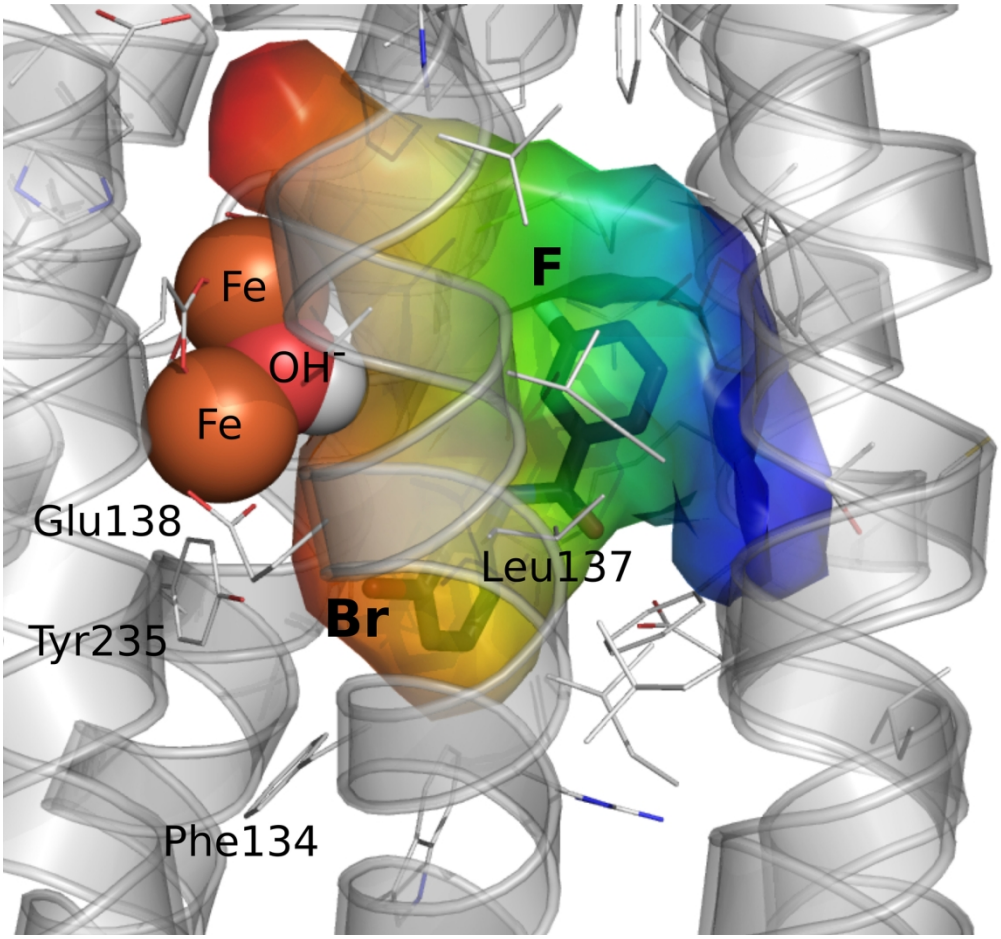

Fig 6. PpAOD structural model and docking of 7j-41. The best docking pose was selected. The color range represents from the aperture of the cavity to the solvent (blue) until the region farthest from that aperture (red). Residues Phe134, Leu137, Glu138 and Tyr235 make up the bromine interaction subsite.

79x73mm (600 x 600 DPI)